Polarized two-photon photoselection in EGFP: Theory and experiment

T. A. Masters, R. J. Marsh, T. S. Blacker, D. A. Armoogum, B. Larijani, and A. J. Bain

Citation: The Journal of Chemical Physics **148**, 134311 (2018); doi: 10.1063/1.5011642
View online: https://doi.org/10.1063/1.5011642
View Table of Contents: http://aip.scitation.org/toc/jcp/148/13
Published by the American Institute of Physics

Polarized two-photon photoselection in EGFP: Theory and experiment

T. A. Masters,[1,2] R. J. Marsh,[1,a)] T. S. Blacker,[1,2] D. A. Armoogum,[1] B. Larijani,[3] and A. J. Bain[1,2,b)]

[1]*Department of Physics and Astronomy, University College London, London WC1E 6BT, United Kingdom*
[2]*CoMPLEX, University College London, London WC1E 6BT, United Kingdom*
[3]*Cell Biophysics Laboratory, Ikerbasque, Basque Foundation for Science and Unidad de Biofisica (CSIC-UPV/EHU), Bilbao, Spain*

(Received 1 November 2017; accepted 13 March 2018; published online 6 April 2018)

In this work, we present a complete theoretical description of the excited state order created by two-photon photoselection from an isotropic ground state; this encompasses both the conventionally measured quadrupolar (K = 2) and the "hidden" degree of hexadecapolar (K = 4) transition dipole alignment, their dependence on the two-photon transition tensor and emission transition dipole moment orientation. Linearly and circularly polarized two-photon absorption (TPA) and time-resolved single- and two-photon fluorescence anisotropy measurements are used to determine the structure of the transition tensor in the deprotonated form of enhanced green fluorescent protein. For excitation wavelengths between 800 nm and 900 nm, TPA is best described by a single element, almost completely diagonal, two-dimensional (planar) transition tensor whose principal axis is collinear to that of the single-photon $S_0 \rightarrow S_1$ transition moment. These observations are in accordance with assignments of the near-infrared two-photon absorption band in fluorescent proteins to a vibronically enhanced $S_0 \rightarrow S_1$ transition.
https://doi.org/10.1063/1.5011642

I. INTRODUCTION

The Green Fluorescent Protein (GFP) has been extensively studied and utilised in a wide range of biophysical applications following its isolation from the *Aquorea victoria* jellyfish.[1–3] In recent years, a large number of mutants have been created to improve fluorescent yield and stability and to provide a spectrum of different absorption and emission maxima.[4,5] Of these, enhanced GFP (EGFP)[6,7] has become one of the most widely used tools for labelling proteins *in vivo*[4,8] and as both a donor and an acceptor in Forster resonance energy transfer (FRET) experiments.[9–12] In parallel to these developments, two-photon excitation has emerged as an important tool in fluorescence spectroscopy and microscopy, affording inherent confocal sectioning and reduced photodamage[13–15] alongside the possibility of enhanced orientational photoselection.[16–20]

Polarized photoselection and fluorescence anisotropy experiments have proved to be valuable tools in the study of both structural changes in proteins[21,22] and the nature of ordered environments such as membranes and vesicles.[23–25] Additionally, these tools have been crucial to highlighting the important role that molecular orientation plays in FRET[26,27] with marked depolarization effects observed in both static and dynamic donor–acceptor systems.[28–30] Intrinsic fluorescence intensity and anisotropy decay dynamics have been studied in wild type GFP and red shifted mutants including EGFP using linearly polarized single- and two-photon excitation.[31–33] Initial fluorescence anisotropies close to 4/10 (single-photon) and 4/7 (two-photon) have been taken as indicating a single-element transition tensor and a parallel emission transition dipole moment.[31] However, the initial two-photon fluorescence anisotropy critically depends on both the structure of the two-photon transition tensor and the molecular frame orientation of the emission transition dipole moment,[17–19] the determination of which require both linearly and circularly polarized absorption and fluorescence anisotropy measurements.

Whilst considerable effort has been directed at determining the mechanism of TPA in fluorescent proteins,[34] a full characterization of the excited states prepared by two-photon excitation has not been attempted. This is of fundamental importance as, in addition to a quadrupolar (rank K = 2) degree of molecular frame and transition dipole alignment, two-photon excitation prepares the higher degree of hexadecapolar (rank K = 4) alignment. Whilst the freely evolving fluorescence anisotropy is sensitive solely to K = 2 transition dipole moment alignment[35–38] and isotropic rotational diffusion ensures that moments of different rank evolve independently,[38,39] in ordered environments these symmetry constraints no longer formally apply.[38] Given the widespread use of polarized two-photon fluorescence techniques in far from isotropic environments,[23,40–42] the development of theory and measurements that provide a complete picture of the excited state order and its evolution are both timely and necessary.

a)Current address: Randall Division of Cell and Molecular Biophysics, New Hunt's House, King's College London, Guy's Campus, London SE1 1UL, United Kingdom.
b)Author to whom correspondence should be addressed: a.bain@ucl.ac.uk

Theoretical treatments calculating the degree of quadrupolar (rank K = 2) alignment as a function of the excitation polarization and transition tensor structure have been presented by a number of groups[17–19,43] as a means of characterising TPA transitions and in the interpretation of time-resolved fluorescence anisotropy measurements of isotropic rotational (K = 2) diffusion. The full degree of angular momentum alignment (K = 2 and K = 4) created by linear and circularly polarized TPA in quantum rotors has been calculated by Bain and McCaffrey using a tensor density matrix approach.[16,35,44] Here, we develop the theory of polarized two-photon photoselection to determine the dependence of both K = 2 and K = 4 degrees of transition dipole alignment on the two-photon tensor structure and the molecular frame orientation of the emission transition dipole moment. Linear and circularly polarized absorption and time-resolved fluorescence anisotropy measurements are undertaken for wavelengths spanning the EGFP two-photon resonance (800-900 nm). Measurement of the initial single-photon fluorescence anisotropy yields the angle between the $S_0 \rightarrow S_1$ absorption and emission transition dipole moments $\mu^{ABS}_{S_0 \rightarrow S_1}$ and $\mu^{EM}_{S_1 \rightarrow S_0}$, the latter being common to both single- and two-photon excited fluorescence. With these data, it is possible to determine the structure of the two-photon transition tensor in relation to $\mu^{ABS}_{S_0 \rightarrow S_1}$ and $\mu^{EM}_{S_1 \rightarrow S_0}$. We find the transition tensor to be almost fully diagonal, dominated by its principal component when the principal axis and $\mu^{ABS}_{S_0 \rightarrow S_1}$ are fully aligned. These results lend weight to the assignment of the near infra-red two-photon absorption band in EGFP as a vibronically enhanced transition between the ground and first excited singlet states.[34,45,46] Finally, we investigate the theoretical dependence of the degree of K = 4 transition dipole alignment on the transition tensor structure and emission transition dipole moment orientation. Our results reveal a different and more marked dependence of the hexadecapolar alignment over the fluorescence anisotropy which is only sensitive to the quadrupolar transition dipole alignment. As will be seen, this leads to a discernible difference in the predicted degree of hexadecapolar alignment depending on whether the principal axis of the transition tensor lies along $\mu^{ABS}_{S_0 \rightarrow S_1}$ or $\mu^{EM}_{S_1 \rightarrow S_0}$, highlighting the utility of measuring both K = 2 and K = 4 alignment in the precise determination of the structure of two-photon transitions in molecular systems.

Fluorescence measurements can only yield information on higher order (K > 2) moments when they are accompanied by an optically induced change in the excited state population and its alignment.[47–56] Determination of the time evolution of the hexadecapolar moments created by TPA therefore requires a quantifiable higher order interaction over that provided by (unperturbed) spontaneous emission. A novel method (theory and experiment) for determining hexadecapolar alignment dynamics in two-photon excited states using time resolved polarized stimulated emission depletion (STED) is set out in the companion paper.[57]

II. CALCULATION OF THE FULL ORIENTATIONAL DISTRIBUTION FUNCTION FOLLOWING TPA

Short-pulsed polarized optical excitation from an initially isotropic (randomly oriented) population of condensed phase fluorescent probes gives rise to an excited state population with a non-isotropic distribution of molecular orientations in the laboratory frame of reference.[16,58,59] Excited state order is most commonly measured through the evolution of the anisotropy of the induced fluorescence which is a direct measure of the degree of emission transition dipole alignment.[38,59,60] In polar co-ordinates, the probability distribution for the emission transition dipole moment is conveniently expressed in terms of a spherical harmonic expansion,[38,59]

$$P_{EX}(\theta,\phi,t) = \sum_{KQ} \left\langle C_{KQ}(t) \right\rangle Y_{KQ}(\theta,\phi). \tag{1}$$

In experiments where the photoselection process possesses an axis of cylindrical symmetry, this defines a common (excitation–detection) laboratory fixed z-axis and the distribution in Eq. (1) reduces to moments for which Q = 0,

$$P_{EX}(\theta,\phi,t) = \sum_{K} \langle C_{K0}(t) \rangle Y_{K0}(\theta,\phi). \tag{2}$$

With single-photon excitation, the excited state distribution contains only the scalar (K = 0) and quadrupolar alignment (K = 2) terms. Conservation of orientational probability requires that $\langle C_{00}(t) \rangle = \sqrt{1/4\pi}$ and the fluorescence anisotropy at time t following excitation is given by[38,59]

$$R(t) = \frac{\langle C_{20}(t) \rangle}{\sqrt{5}\langle C_{00} \rangle} = \frac{\langle \alpha_{20}(t) \rangle}{\sqrt{5}}. \tag{3}$$

With two-photon absorption, the emission transition dipole moment distribution contains the additional hexadecapolar alignment (K = 4) term,

$$P^{TPA}_{EX}(\theta,\phi,t) = \frac{1}{\sqrt{4\pi}} \left[Y_{00}(\theta,\phi) + \langle \alpha_{20}(t) \rangle Y_{20}(\theta,\phi) + \langle \alpha_{40}(t) \rangle Y_{40}(\theta,\phi) \right]. \tag{4}$$

The degree of hexadecapolar alignment $\langle \alpha_{40}(0) \rangle$ created by TPA and its evolution cannot be measured directly by spontaneous emission[36,47] and has to date been largely neglected by theoretical treatments of TPA. Measurements of the polarization dependence (linear vs. circular) of the TPA cross section (a scalar measurement) have been successfully combined with time-resolved fluorescence anisotropy data to determine the transition tensor structure and emission dipole moment orientation.[33,43] Hexadecapolar alignment is not a silent partner and is observable through nonlinear techniques such as fluorescence recovery after photobleaching,[54–56] ground state depletion,[53] and STED.[47–52]

The rationale for the theoretical work presented in this paper is as follows: we first present the general theory of the polarization dependence of the TPA cross section using generalized spherical co-ordinates to describe the laboratory frame measurement and Cartesian tensors to characterize the interaction between the input fields and the molecular fixed components of the two-photon transition tensor, introducing the basic theoretical concepts that will be exploited later. We then develop a general method for calculating the initial expectation values for $\cos^2\theta$ and $\cos^4\theta$ emission transition dipole alignment following TPA, yielding expressions for the transition tensor and molecular frame emission dipole moment dependence of $\langle \alpha_{20}(0) \rangle$ and $\langle \alpha_{40}(0) \rangle$, which [in the case of $\langle \alpha_{20}(0) \rangle$] can be tested against existing theoretical models.[18,19,43]

A. Scalar terms: Polarization dependence of the TPA cross section

Both spherical[18,61] and Cartesian[62,63] tensor formalisms have been developed to treat polarized fluorescence following TPA in molecular systems. In experiments involving different laboratory frame excitation-detection schemes (e.g., fluorescence anisotropy following linear and circular polarized TPA), the transformation between co-ordinate systems is most effectively achieved using spherical tensors as the relationship between fluorescence observables and expectation values are particularly concise, such as in Eq. (3). Employing a spherical tensor formalism for TPA, the orientation-dependent transition probability for two identical photons with electric field polarization ê can be written as[18,61]

$$A(\Omega) = \left|\hat{e}\cdot\underline{S}\cdot\hat{e}\right|^2, \tag{5}$$

where $\underline{S}$ is a second rank tensor describing the angular properties of the two-photon transition between initial and final states $|i\rangle$ and $|f\rangle$ connected by intermediate states $|n\rangle$ with linewidth Γ_n and detuning $\Delta\nu_{n\alpha}$ from the excitation frequency ν_α, and $\Omega(\alpha, \beta, \gamma)$ denotes the molecular frame orientation in the laboratory frame,

$$\underline{S} \propto \sum_n \left(\frac{\langle f|\,\mu\,|n\rangle\langle n|\,\mu\,|i\rangle}{\Delta\nu_{n\alpha} + i\Gamma_n}\right). \tag{6}$$

For the absorption of two identical photons, Eq. (5) can be written as

$$A(\Omega) = \left|\underline{T}\cdot\underline{S}\right|^2. \tag{7}$$

The excitation polarization tensor $\underline{T}$ is given by the direct product of the photon polarization vectors,

$$\underline{T} = (\hat{e}\otimes\hat{e}) = \sum_{lm} T^l_m(Lab). \tag{8}$$

Expressing $\underline{S}$ and $\underline{T}$ as spherical tensors, the scalar product in Eq. (7) becomes

$$\underline{T}\cdot\underline{S} = \sum_{lm} T^l_m(lab)\,S^l_{-m}(lab)\,(-1)^m. \tag{9}$$

The transition tensor $\underline{S}$ is determined by molecular frame quantities (i.e., the products of the single-photon molecular transition dipole matrix elements). However the scalar product in Eq. (7) is expressed in the laboratory frame where the components of $\underline{T}$ are determined by the excitation polarization vectors. The components of $\underline{S}$ in the laboratory frame are obtained by an Euler rotation $D(\Omega_{LM})$ that connects the laboratory and molecular reference frames,[64]

$$S^l_{-m}(lab) = \sum_n S^l_n(mol) D^l_{n-m}(\Omega_{LM}), \tag{10}$$

where $D^l_{n-m}(\Omega_{LM})$ is the Euler rotation matrix element for the rotation.[64] With this substitution, the scalar product becomes

$$\underline{T}\cdot\underline{S} = \sum_{l,m,n} T^l_m(lab)\,D^l_{n-m}(\Omega_{LM})\,S^l_n(mol)\,(-1)^m. \tag{11}$$

The orientation dependent transition probability is thus

$$A(\Omega) = \sum_{l\,l'm\,m'nn'} T^l_m(lab)\,T^{l'}_{m'}(lab)^* D^l_{n-m}(\Omega_{LM})\,D^{l'}_{n'-m'}(\Omega_{LM})^* \times S^l_n(mol)\,S^{l'*}_{n'}(mol)\,(-1)^{m+m'}. \tag{12}$$

After some manipulation and the contraction of rotation matrix element products,[18,58,65] $A(\Omega)$ can be written in terms of the rotation matrix element expansion,

$$A(\Omega) = \sum_{KQN} A^K_{NQ} D^K_{NQ}(\Omega_{LM}). \tag{13}$$

The moments of this are given by

$$A^K_{QN} = (2K+1)(-1)^N \times \sum_{ll'mm'nn'} \left[\begin{pmatrix} l & l' & K \\ m & -m' & -Q\end{pmatrix}\begin{pmatrix} l & l' & K \\ -n & n' & -N\end{pmatrix} \times T^l_m(lab)\,T^{l'}_{-m'}(lab)\,S^l_n(mol)\,S^{l'}_{-n'}(mol)\right]. \tag{14}$$

For linearly polarized TPA, $\boldsymbol{l}$ and $\boldsymbol{l'}$ can take values of 0 and 2.[64] Cylindrical symmetry about the excitation polarization vector means $\boldsymbol{m}$, $\boldsymbol{m'}$ and $\boldsymbol{Q}$ are zero, odd values of $\boldsymbol{K}$ are thus forbidden restricting $\boldsymbol{K}$ to values of 0, 2, and 4.[64] The allowed values of N depend on the elements of the molecular frame transition tensor $\underline{S}$,

$$A^K_{N0}(linear) = (2K+1)(-1)^N \times \sum_{l,l',n,n'} \left[\begin{pmatrix} l & l' & K \\ 0 & 0 & 0\end{pmatrix}\begin{pmatrix} l & l' & K \\ -n & n' & -N\end{pmatrix} \times T^l_0(lab)\,T^{l'}_0(lab)\,S^l_n(mol)\,S^{l'}_{-n'}(mol)\right]. \tag{15}$$

For TPA with circularly polarized light, the only non-zero excitation tensor product is $T^2_2(lab)\,T^2_{-2}(lab)$ and the moments of $A(\Omega)$ are given by

$$A^K_{N0}(circ) = (2K+1)(-1)^N T^2_2(lab)\,T^2_{-2}(lab) \times \sum_{n,n'} \left[\begin{pmatrix} 2 & 2 & K \\ 2 & -2 & 0\end{pmatrix}\begin{pmatrix} 2 & 2 & K \\ -n & n' & -N\end{pmatrix} \times S^2_n(Mol)\,S^2_{-n}(Mol)\right]. \tag{16}$$

It should be noted that in contrast to linearly polarized TPA, the axis of cylindrical symmetry with circularly polarized excitation is the propagation direction of the exciting light.

The TPA cross section $\sigma^{(2)}$ is proportional to the scalar coefficient A^0_{00}.[18,19,43] As a result of the different excitation polarization tensors, linear and circularly polarized TPA cross sections sample different combinations of the elements of $\underline{S}$. The ratio of linear to circularly polarized TPA absorption Ω_{ABS} has been used as a means of determining the structure of $\underline{S}$ and the symmetry of the electronic states involved in TPA.[18,65,66] The TPA cross sections for linear and circularly polarized TPA are

$$\sigma^{(2)}_{LIN} = Const \times \left[T^0_0(lab)^2 S^0_0(mol)^2 + T^2_0(lab)^2 \sum_n \frac{(-1)^n}{5} S^2_n(mol)\,S^2_{-n}(mol)\right], \tag{17}$$

$$\sigma^{(2)}_{CIRC} = Const \times T^2_2\,(lab)\,T^2_{-2}\,(lab) \times \sum_n \frac{(-1)^n}{5} S^2_n\,(mol)\,S^2_{-n}\,(mol)\,. \tag{18}$$

The relationship between the spherical and Cartesian components U^l_m and $U_{ij}(i,j=x,y,z)$ of a second rank tensor $\underline{U}$ can be calculated using standard angular momentum methods[18] and can be expressed in matrix form as[18,61,66]

$$\begin{bmatrix} S^0_0 \\ S^2_{-2} \\ S^2_{-1} \\ S^2_0 \\ S^2_1 \\ S^2_2 \end{bmatrix} = \begin{bmatrix} -\frac{1}{\sqrt{3}} & 0 & 0 & 0 & -\frac{1}{\sqrt{3}} & 0 & 0 & 0 & -\frac{1}{\sqrt{3}} \\ \frac{1}{2} & \frac{-i}{2} & 0 & \frac{-i}{2} & \frac{1}{2} & 0 & 0 & 0 & 0 \\ 0 & 0 & \frac{1}{2} & 0 & 0 & \frac{-i}{2} & \frac{1}{2} & \frac{-i}{2} & 0 \\ -\frac{1}{\sqrt{6}} & 0 & 0 & 0 & -\frac{1}{\sqrt{6}} & 0 & 0 & 0 & \sqrt{\frac{2}{3}} \\ 0 & 0 & -\frac{1}{2} & 0 & 0 & -\frac{i}{2} & -\frac{1}{2} & -\frac{i}{2} & 0 \\ \frac{1}{2} & \frac{i}{2} & 0 & \frac{i}{2} & -\frac{1}{2} & 0 & 0 & 0 & 0 \end{bmatrix} \times \begin{bmatrix} S_{XX} \\ S_{XY} \\ S_{XZ} \\ S_{YX} \\ S_{YY} \\ S_{YZ} \\ S_{ZX} \\ S_{ZY} \\ S_{ZZ} \end{bmatrix}. \tag{19}$$

Inserting the expressions for the laboratory frame polarization tensors for linear and circular polarizations, the TPA cross section ratio Ω_{ABS} is given by

$$\Omega_{ABS} = \frac{\sigma^{(2)}_{CIRC}}{\sigma^{(2)}_{LIN}} = \frac{(T_{XY})^2 \sum_n \frac{(-1)^n}{5} S^2_n\,(mol)\,S^2_{-n}\,(mol)}{(T_{ZZ})^2 \left[\frac{1}{3} S^0_0 (mol)^2 + \frac{2}{3} \sum_n \frac{(-1)^n}{5} S^2_n\,(mol)\,S^2_{-n}\,(mol)\right]}. \tag{20}$$

As $(T_{XY})^2 = (T_{YX})^2 = (T_{ZZ})^2$, Eq. (20) becomes

$$\Omega_{ABS} = \frac{3 \sum_n (-1)^n S^2_n\,(Mol)\,S^2_{-n}\,(Mol)}{5S^0_0(Mol)^2 + 2\sum_n (-1)^n S^2_n\,(Mol)\,S^2_{-n}\,(Mol)}. \tag{21}$$

High resolution X-ray crystallography studies indicate that the chromophores in both EGFP and GFP are planar.[67,68] For a planar (XY) transition tensor, the $S^2_{\pm 1}\,(mol)$ elements from Eq. (19) are necessarily zero and Eq. (21) simplifies to

$$\Omega_{ABS} = \frac{3\left(S^2_0\,(mol)\,S^2_0\,(mol) + 2S^2_2\,(mol)\,S^2_{-2}\,(mol)\right)}{5S^0_0(mol)^2 + 2\left(S^2_0\,(mol)\,S^2_0\,(mol) + 2S^2_2\,(mol)\,S^2_{-2}\,(mol)\right)}. \tag{22}$$

Dropping the mol suffix and using the relations in Eq. (19), we have

$$\Omega_{ABS} = \frac{(S_{XX}+S_{YY})^2 + 3(S_{XX}-S_{YY})^2 + 3(S_{XY}+S_{YX})^2}{2(S_{XX}+S_{YY})^2 + (S_{XX}-S_{YY})^2 + (S_{XY}+S_{YX})^2}. \tag{23}$$

For the absorption of two identical photons, $S_{XY} = S_{YX}$. Then, dividing the numerator and denominator by ${S_{XX}}^2$ yields

$$\Omega_{ABS} = \frac{(1+S)^2 + 3(1-S)^2 + 12D^2}{2(1+S)^2 + (1-S)^2 + 2D^2}, \tag{24}$$

where $S = \mathrm{S_{YY}}/S_{XX}$ and $D = \mathrm{S_{XY}}/S_{XX}$, in agreement with previous calculations.[18,19,43,58]

B. Fluorescence anisotropy: Quadrupolar alignment

Expressions for the fluorescence anisotropy resulting from two-photon excitation have been determined by a number of groups via the calculation of the emission intensities for light polarized parallel and perpendicular to the excitation polarization.[38] We now present a more direct approach to calculation of the fluorescence anisotropy which we later employ to calculate the degree of hexadecapolar alignment which itself has no corresponding direct linear measurement [cf. Eq. (3)].

The initial value of the fluorescence anisotropy can be calculated from the expectation value of $\cos^2\theta$ where θ is the angle between the laboratory Z axis and the emission transition dipole moment. In a spherical harmonic expansion, $\cos^2\theta$ is given by

$$\cos^2\theta = \frac{\sqrt{4\pi}}{3}\left[Y_{00}\,(\theta,\phi) + \frac{2}{\sqrt{5}} Y_{20}\,(\theta,\phi)\right]. \tag{25}$$

This is related to the scalar product of the emission transition dipole moment μ_{LAB} and the emission polarization vector E^Z_{LAB} through

$$\cos^2\theta = c \times \left|E^Z_{LAB} \cdot \mu_{LAB}\right|^2, \tag{26}$$

where $\boldsymbol{c}$ is a constant of proportionality. Starting with the standard spherical tensor expression for $\cos^2\theta$, we have

$$\cos^2\theta = c\left|\sum_n T^1_0\,(lab)\,\mu^1_n D^1_{n0}\,(\Omega)\right|^2, \tag{27}$$

where $T^1_0 \equiv E_Z$. Following a similar approach to that in Eqs. (12)–(14), the rotation matrix products are contracted to give

$$\left|E^Z_{LAB} \cdot \mu_{LAB}\right|^2 = c^2\left(T^1_0\,(lab)\right)^2 \sum_{LN} B^L_{N0} D^L_{N0}\,(\Omega), \tag{28}$$

with

$$B^L_{N0} = \sum_{nn'}\left[\begin{array}{l}\mu^1_n\,(mol)\,\mu^1_{-n'}\,(mol)\\ \\ \times\begin{pmatrix}1 & 1 & L\\ 0 & 0 & 0\end{pmatrix}\begin{pmatrix}1 & 1 & L\\ n & -n' & -N\end{pmatrix}(2L+1)\,(-1)^N\end{array}\right]. \tag{29}$$

The B^L_{N0} terms (L = 0, 2; N = 0 ± 2) contain the molecule-fixed transition dipole moment terms and $D^L_{-N0}\,(\Omega)$ is the Euler rotation matrix that connects the laboratory and molecular frames. For a planar (XY) transition in the molecular frame of reference, we have[65]

$$\begin{aligned} B^0_{00} &= \frac{1}{3}\left(\mu^2_X + \mu^2_Y\right),\ B^2_{00} = \frac{-1}{3}\left(\mu^2_X + \mu^2_Y\right),\\ B^2_{\pm 20} &= \sqrt{\frac{1}{6}}\left[\left(\mu^2_X - \mu^2_Y\right) \pm 2i\mu_X\mu_Y\right]. \end{aligned} \tag{30}$$

We now determine the expectation value

$$\int A\,(\Omega)\cos^2\theta d\Omega, \tag{31}$$

where $A(\Omega)$ is given by the cylindrically symmetric (laboratory frame) form of Eq. (13),

$$A\,(\Omega) = \sum_{KN} A^K_{N0} D^K_{N0}\,(\Omega_{LM}), \tag{32}$$

Inserting (28) and (32) into (31) gives

$$\int A\,(\Omega)\cos^2\theta d\Omega = c^2 \sum_{\substack{LN'\\K}} A^K_{N0} B^L_{N'0} \int D^K_{N0}\,(\Omega)\, D^L_{N'0}\,(\Omega)\, d\Omega. \tag{33}$$

The orthogonality relation for rotation matrices imposes the following restriction:[64]

$$\int D^K_{N0}\,(\Omega)\, D^L_{N'0}\,(\Omega)\, d\Omega = \frac{8\pi^2}{2K+1}\delta_{KL}\delta_{N-N'}(-1)^N. \tag{34}$$

As a result, the expectation value of $\cos^2\theta$ is

$$\int A\,(\Omega)\cos^2\theta d\Omega = c^2\frac{8\pi^2}{2K+1}\sum_{KN} A^K_{N0} B^K_{-N0}(-1)^N. \tag{35}$$

The expectation values of Y_{00} and Y_{20} are $\langle C_{00}\rangle$ and $\langle C_{20}\rangle$.[18] Combining Eqs. (25) and (35) gives

$$\frac{\sqrt{4\pi}}{3}\left[\langle C_{00}\rangle + \frac{2}{\sqrt{5}}\langle C_{20}\rangle\right] = c^2\frac{8\pi^2}{2L+1}\sum_{KN} A^L_{N0} B^L_{-N0}(-1)^N. \tag{36}$$

The degree of quadrupolar alignment is thus

$$\langle\alpha_{20}\rangle = \frac{\langle C_{20}\rangle}{\langle C_{00}\rangle} = \frac{\sqrt{5}}{10}\frac{\sum_N A^2_{N0}B^2_{-N0}(-1)^N}{A^0_{00}B^0_{00}}. \tag{37}$$

From Eq. (3), the fluorescence anisotropy is

$$R = \frac{1}{10}\frac{\sum_N A^2_{-N0}B^2_{-N0}(-1)^N}{A^0_{00}B^0_{00}}. \tag{38}$$

From Eqs. (14) and (16), the second rank moments of $A(\Omega)$ for linear and circularly polarized excitation are given by

$$A^2_{N0}(lin) = 5(-1)^N\left[\begin{array}{l}\frac{2}{\sqrt{5}}T^2_0\,(lab)\,T^0_0\,(lab)\sum_n\begin{pmatrix}2 & 0 & 2\\ -n & 0 & -N\end{pmatrix}S^l_n\,(mol)\,S^0_0\,(mol)\\ \\ +\sqrt{\frac{2}{35}}T^2_0\,(lab)\,T^2_0\,(lab)\sum_{n,n'}\begin{pmatrix}2 & 2 & 2\\ -n & n' & -N\end{pmatrix}S^2_n\,(mol)\,S^2_{n'}\,(mol)\end{array}\right], \tag{39}$$

$$A^2_{N0}(circ) = 5(-1)^N\begin{pmatrix}2 & 2 & 2\\ 2 & -2 & 0\end{pmatrix}T^2_2\,(lab)\,T^2_{-2}\,(lab)\sum_{n,n'}\left[\begin{array}{l}\begin{pmatrix}2 & 2 & 2\\ -n & n' & -N\end{pmatrix}\\ \\ \times S^2_n\,(mol)\,S^2_{-n}\,(mol)\end{array}\right]. \tag{40}$$

The allowed two-photon transition and emission dipole tensor elements for planar (XY) absorption with a co-planar emission transition dipole moment are set out in Table I. After substitution of these values into Eqs. (38)–(40), the initial fluorescence anisotropies for linear and circularly polarized TPA are given by

$$R_L(0) = \frac{1}{7}\left[1 + \frac{9\left(1-S^2\right)\left(\cos^2\theta_M - \sin^2\theta_M\right) + 4\,(1+S)\,D\sin\theta_M\cos\theta_M}{2(1+S)^2 + (1-S)^2 + 4D^2}\right], \tag{41}$$

$$R_C(0) = \frac{1}{7}\left[\frac{(1+S)^2 - 3\left[(1-S)^2 + 4D^2\right] - 6\left[\begin{array}{l}\left(\cos^2\theta_M - \sin^2\theta_M\right)\left(1-S^2\right)\\ +4D\,(1+S)\sin\theta_M\cos\theta_M\end{array}\right]}{(1+S)^2 + 3(1-S)^2 + 12D^2}\right], \tag{42}$$

where $\cos\theta_M = \mu_X/\sqrt{\left(\mu_X^2+\mu_Y^2\right)}$, $\sin\theta_M = \mu_Y/\sqrt{\left(\mu_X^2+\mu_Y^2\right)}$, and θ_M is the angle made by the emission transition dipole with respect to the X direction in the molecular frame, taken to be that corresponding to the principal diagonal tensor element (S_{XX}). For a transition tensor with a single element S_{XX}, Eqs. (41) and (42) take on a particularly simple form

$$R_L(0) = \frac{4}{7}\left(\frac{3\cos^2\theta_M - 1}{2}\right), \tag{43}$$

$$R_C(0) = -\left(\frac{3\cos^2\theta_M - 1}{7}\right). \tag{44}$$

Experimental measurements are defined in a co-ordinate system in which the laboratory Z axis is defined by the natural quantization (cylindrical symmetry) axis of the excitation process. As a result, the measurement $I_{\parallel}(t) + 2I_{\perp}(t)$ contains no alignment contributions. The laboratory Z axes are orthogonal for linear and circularly polarized TPA as shown in Fig. 1. An alternative approach retains a common laboratory fixed frame of reference for the measurement of the linearly polarized emission anisotropy in which the Z axis is defined by that of the linear polarization vector of the excitation light.[36–38] Denoting this emission anisotropy as $R_C{}'$, the two circularly polarized excitation anisotropies are related by

$$R'_C = -R_C/(1+R_C). \tag{45}$$

For a single-element transition tensor with $\theta_M = 0$, we have $R_L(0) = 4/7$, $R_C(0) = -2/7$, and $R'_C(0) = 2/5$.

C. Hexadecapolar alignment

Unlike the quadrupolar (second rank) degrees of molecular alignment, higher rank moments of the excited state distribution do not contribute directly to spontaneous emission[47–52] but affect the changes to the intensity and polarization of spontaneous emission as a result of stimulated emission depletion.[36–38,58] Single and multiphoton absorption with linearly or circularly polarized light leads to the creation of an excited state distribution with cylindrical symmetry about the relevant laboratory fixed quantization (Z) axis.[64] The degree of

TABLE I. Transition tensor and spontaneous emission transition dipole moment elements for planar TPA and coplanar spontaneous emission.

	Linear polarization ↑↑	Circular polarization ↻↺	$\cos^2\theta$ dipole moment tensor elements
	$A^L_{N0}(lin)\times(T_{ZZ}S_{XX})^2$	$A^I_{N0}(circ)\times(T_{XY}S_{XX})^2$	B^I_{N0}
$L=0$ $N=0$	$2(1+S)^2+(1-S)^2+4D^2$	$(1+S)^2+3(1-S)^2+12D^2$	$\frac{1}{3}\left(\mu_X^2+\mu_Y^2\right)$
$L=2$ $N=0$	$\frac{-2\left[2(1+S)^2+(1-S)^2+4D^2\right]}{21}$	$\frac{-(1+S)^2+3(1-S)^2+12D^2}{21}$	$\frac{-1}{3}\left(\mu_X^2+\mu_Y^2\right)$
$L=2$ $N=\pm2$	$\frac{\left(1-S^2\right)\pm2iD(1+S)}{7\sqrt{6}}$	$\frac{2\left(1-S^2\right)\pm4iD(1+S)}{7\sqrt{6}}$	$\frac{1}{\sqrt{6}}\left[\left(\mu_X^2-\mu_Y^2\right)\pm2i\mu_X\mu_Y\right]$
$(T_{ZZ})^2=(T_{XY})^2=(T_{YX})^2$ $S=S_{YY}/S_{XX}$ $D=S_{XY}(=S_{YX})/S_{XX}$			

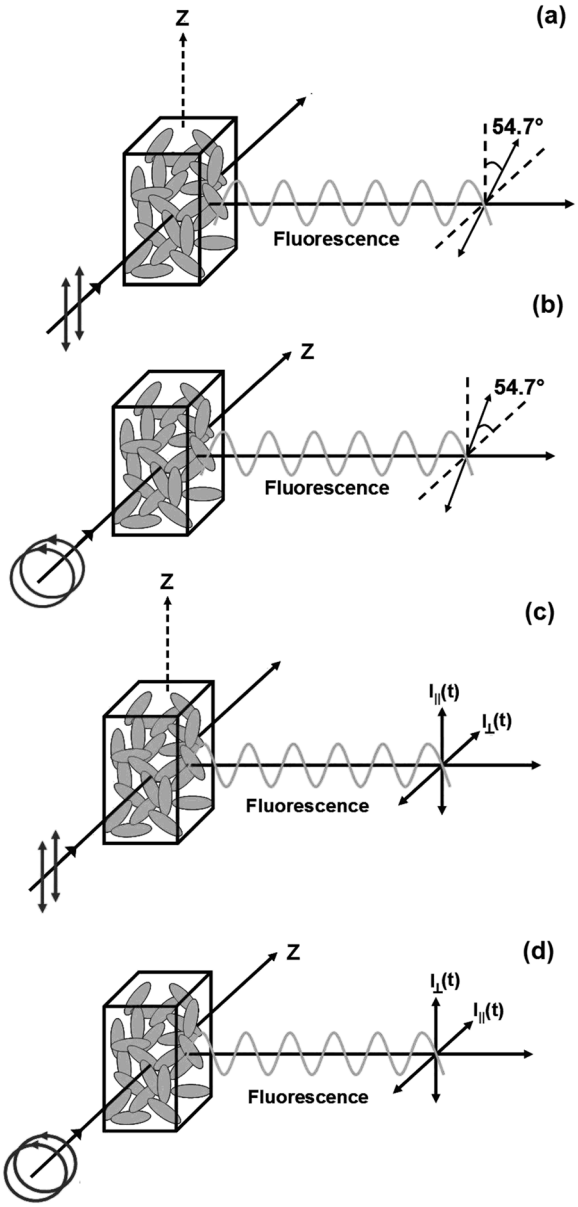

FIG. 1. The 90° excitation-detection geometry employed to determine the two-photon transition tensor. [(a) and (b)] To determine Ω, time averaged emission with linearly and circularly polarized excitation is collected at 54.7° to the prevailing symmetry axis. For determination of (c) $R_L(0)$ and (d) $R_C(0)$, initial anisotropies for linearly and circularly polarized light are measured by collection of intensity parallel ($I_{\parallel}(t)$) and perpendicular ($I_{\perp}(t)$) to the prevailing axis of cylindrical symmetry.

cylindrically symmetric quadrupolar and hexadecapolar transition dipole moment alignment can be related to the expectation value of $\cos^4\theta$. In a spherical harmonic expansion, $\cos^4\theta$ is given by

$$\cos^4\theta = \frac{\sqrt{4\pi}}{5}\left[Y_{00}(\theta,\phi) + \frac{20}{7\sqrt{5}}Y_{40}(\theta,\phi) + \frac{8}{21}Y_{40}(\theta,\phi)\right] = C \times \left|E^Z_{LAB}\cdot\mu_{LAB}\right|^4. \quad (46)$$

Taking the square of Eq. (28),

$$\left|E^Z_{LAB}\cdot\mu_{LAB}\right|^4 = \sum_{\substack{LN\\L'N'}} B^L_{N0}B^{L'}_{N'0}D^L_{N0}(\Omega)\,D^{L'}_{N'0}(\Omega). \quad (47)$$

The product of rotation matrices can be contracted as above giving

$$\cos^4\theta = C\sum_{\substack{LNL'N'\\K''N''}} B^L_{N0}B^{L'}_{N'0}(2K''+1)\begin{pmatrix} L & L' & K''\\ N & N' & -N''\end{pmatrix} \times \begin{pmatrix} L & L' & K''\\ 0 & 0 & 0\end{pmatrix} D^{K''}_{N''0}(\Omega)(-1)^{N''}. \quad (48)$$

This can be written as

$$\cos^4\theta = C\sum_{KN''} F^K_{N''0}D^K_{N''0}(\Omega). \quad (49)$$

From the symmetry constraints of the 3j symbols[64] given L, L′ = 0, 2 and N, N′ = 0 ± 2, the allowed values of K and N″ are K = 0, 2, 4; N″ = 0 ± 2 ±4. The allowed $F^K_{N''0}$ coefficients and their dependence on the transition dipole element terms are shown in Table II.

The expectation value of $\cos^4\theta$ is

$$\left\langle\cos^4\theta\right\rangle = \int A(\Omega)\cos^4\theta d\Omega. \quad (50)$$

Substituting Eqs. (46) and (49) into Eq. (50) gives

$$\left\langle\cos^4\theta\right\rangle = \frac{\sqrt{4\pi}}{5}\left[\langle C_{00}\rangle + \frac{20}{7\sqrt{5}}\langle C_{20}\rangle + \frac{8}{21}\langle C_{40}\rangle\right] = C\sum_{\substack{K'N'\\KN''}} A^{K'}_{N'0}F^K_{N''0}\int D^{K'}_{N'0}(\Omega)\,D^K_{N''0}(\Omega)\,d\Omega. \quad (51)$$

From the orthogonality relation for rotation matrices,[64] we have

$$\int A(\Omega)\cos^4\theta d\Omega = C\frac{8\pi^2}{2K+1}\sum_{KN} A^K_{-N0}F^K_{N0}(-1)^N. \quad (52)$$

Equating terms in Eqs. (51) and (52), $\langle C_{00}\rangle$ and $\langle C_{40}\rangle$ are given by

$$\langle C_{40}\rangle = \frac{35}{6}C\pi^{\frac{3}{2}}\sum_N A^4_{-N0}F^4_{N0}(-1)^N, \quad (53)$$

$$\langle C_{00}\rangle = 20C\pi^{\frac{3}{2}}A^0_{00}F^0_{00}. \quad (54)$$

The degree of hexadecapolar dipole alignment is therefore

$$\langle\alpha_{40}\rangle = \frac{7}{24}\left[\frac{\sum_N A^4_{N0}F^4_{-N0}(-1)^N}{A^0_{00}F^0_{00}}\right]. \quad (55)$$

Substitution for the $A^4_{N0}F^4_{-N0}$ terms in Table II yields

$$\langle\alpha_{40}\rangle = \frac{3}{56} + \frac{\begin{bmatrix} 20\begin{pmatrix}(\cos^4\theta_M - \sin^4\theta_M)(1-S^2)\\ +4D(1+S)\cos\theta_M\sin\theta_M\end{pmatrix} \\ +35\begin{pmatrix}(1-8\cos^2\theta_M\sin^2\theta_M)((1-S)^2-4D^2)\\ +16D(1-S)\cos\theta_M\sin\theta_M(\cos^2\theta_M-\sin^2\theta_M)\end{pmatrix}\end{bmatrix}}{56(2(1+S)^2+(1-S)^2+4D^2)}. \tag{56}$$

Simplifying,

$$\langle\alpha_{40}\rangle = \frac{3}{56} + \frac{\begin{bmatrix} 20\left((2\cos^2\theta_M-1)(1-S^2)+4D(1+S)\cos\theta_M\sin\theta_M\right) \\ +35\begin{pmatrix}(1-8\cos^2\theta_M\sin^2\theta_M)((1-S)^2-4D^2)\\ +16D(1-S)\cos\theta_M\sin\theta_M(\cos^2\theta_M-\sin^2\theta_M)\end{pmatrix}\end{bmatrix}}{56(2(1+S)^2+(1-S)^2+4D^2)}. \tag{57}$$

For a single-element transition tensor, S and D are zero and Eq. (57) reduces to

$$\langle\alpha_{40}\rangle = \frac{1}{21}\left(35\cos^4\theta_M - 30\cos^2\theta_M + 3\right) = \frac{8}{21}P_4(\cos\theta_M). \tag{58}$$

This corresponds to the degree of hexadecapolar transition dipole alignment arising from a pure $\cos^4\theta$ excitation probability [Eq. (46)] modified by a molecular frame rotation θ_M. This has maximum positive and negative values of 8/21 and −8/49, respectively. Plots of the variation in $\langle\alpha_{20}\rangle/\sqrt{5}$ and $\langle\alpha_{40}\rangle$ with S for a diagonal transition tensor ($D = 0$) with a parallel emission transition dipole moment ($\theta_M = 0°$) are shown in Fig. 2(a). This is contrasted in Fig. 2(b) which shows the off-diagonal transition tensor dependence (D) on these quantities in a planar transition with $S = 1$ and correspondingly equal projection of the emission transition dipole moment on the in plane X and Y axes ($\theta_M = 45°$). From Fig. 2(a), the maximum value of $\langle\alpha_{20}\rangle/\sqrt{5} \equiv R_L(0)$ is not 4/7 (S = 0) but $(4+9\sqrt{2})/28$ (≈0.5974) for $S = -3 + (2\sqrt{2})$ (≈−0.0858). The possibility that $R_L(0)$ can exceed the value of 4/7 (≈0.5714) has been noted previously.[18] However, for $\langle\alpha_{40}\rangle$, the S dependence is more pronounced. For $S = 0$, $\langle\alpha_{40}\rangle = 8/21$ (≈0.3809), increasing to $(41 + 5\sqrt{57})/112$ (≈0.7031) for $S = (1 - 3\sqrt{(19/3)})/2$ (≈−0.7583). For a planar transition where $S = 1$, the variation in $\langle\alpha_{40}\rangle$ with D [Fig. 2(b)] is correspondingly more pronounced than that of the quadrupolar alignment with $\langle\alpha_{40}\rangle$ varying between $(41+5\sqrt{(57)})/112$ (≈0.7031) and $(41-5\sqrt{(57)})/112$ (≈0.0290). The measurement of the degree of hexadecapolar alignment therefore provides an additional and potentially more sensitive probe of the structure of the two-photon transition tensor.

III. EXPERIMENTAL PROCEDURE

Recombinant EGFP samples were prepared to 1-4 μM concentration in pH 11 buffer (50 mM Tris, 300 mM NaCl) using methods described previously.[28] Two-photon excitation wavelengths between 800 and 900nm were provided by an

TABLE II. Fourth rank transition tensor and transition dipole moment elements.

	A^I_{J0}	F^I_{J0}
$I = 0$ $J = 0$	$\frac{(T_{ZZ})^2}{15}\begin{bmatrix}2(S_{XX}+S_{YY})^2\\ +(S_{XX}-S_{YY})^2+4(S_{XY})^2\end{bmatrix}$	$\frac{\left(T^1_0\right)^4}{5}\left[\left(\mu_X^4+\mu_Y^4\right)+2\mu_X^2\mu_Y^2\right]$ $=\frac{\left(T^1_0\right)^4}{5}\left(\mu_X^2+\mu_Y^2\right)^2=\frac{\left(T^1_0\right)^4}{5}\lvert\mu\rvert^4$
$I = 4$ $J = 0$	$\frac{(T_{ZZ})^2}{35}\begin{pmatrix}2(S_{XX}+S_{YY})^2\\ +(S_{XX}-S_{YY})^2+4(S_{XY})^2\end{pmatrix}$	$F^4_{00}=\frac{3\left(T^1_0\right)^4}{35}\lvert\mu\rvert^4$
$I = 4$ $J = \pm2$	$-(T_{ZZ})^2\frac{2}{7}\sqrt{\frac{1}{10}}(S_{XX}+S_{YY})$ $\times[(S_{XX}-S_{YY})\pm 2iS_{XY}]$	$-\left(T^1_0\right)^4\frac{2}{7}\sqrt{\frac{1}{10}}\begin{bmatrix}\left(\mu_X^4-\mu_Y^4\right)\\ \pm2i\mu_X\mu_Y\left(\mu_X^2+\mu_Y^2\right)\end{bmatrix}$ $=-\left(T^1_0\right)^4\frac{2}{7}\sqrt{\frac{1}{10}}\lvert\mu\rvert^4\begin{bmatrix}\left(\cos^2\theta-\sin^2\theta\right)\\ \pm2i\sin\theta\cos\theta\end{bmatrix}$
$I = 4$ $J = \pm4$	$\frac{(T_{ZZ})^2}{\sqrt{70}}\begin{bmatrix}(S_{XX}-S_{YY})^2-4(S_{XY})^2\\ \pm4iS_{XY}(S_{XX}-S_{YY})\end{bmatrix}$	$\left(T^1_0\right)^4\sqrt{\frac{1}{70}}\begin{bmatrix}\left(\mu_X^2-\mu_Y^2\right)^2-4\mu_X^2\mu_Y^2\\ \pm4i\mu_X\mu_Y\left(\mu_X^2-\mu_Y^2\right)\end{bmatrix}$ $=\left(T^1_0\right)^4\sqrt{\frac{1}{70}}\lvert\mu\rvert^4\begin{bmatrix}\left(1-8\cos^2\theta\sin^2\theta\right)\\ \pm4i\cos\theta\sin\theta\left(\cos^2\theta-\sin^2\theta\right)\end{bmatrix}$

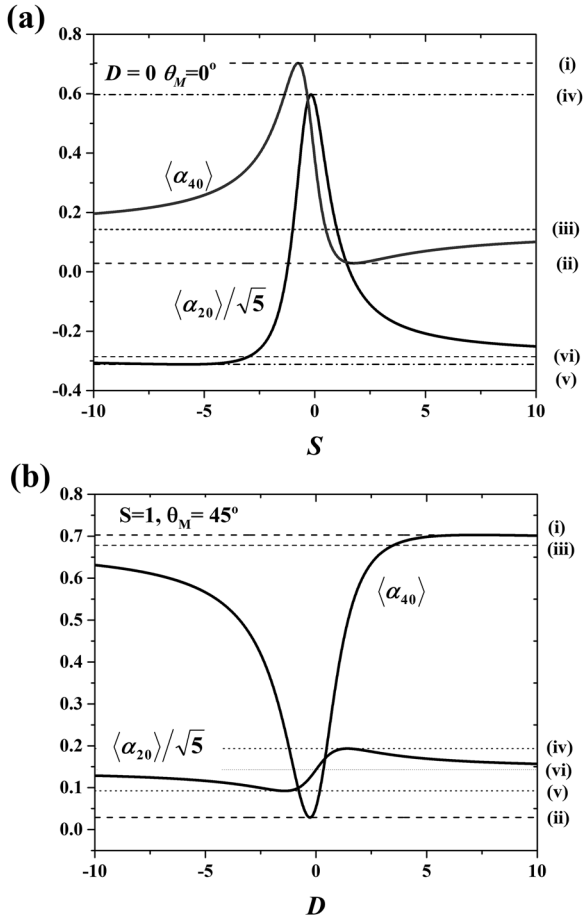

FIG. 2. (a) Variation in $\langle\alpha_{20}\rangle/\sqrt{5}$ and $\langle\alpha_{40}\rangle$ with $S(S_{YY}/S_{XX})$ for TPA characterized by a diagonal transition tensor ($D = 0$) and an emission transition dipole moment parallel to the molecular X axis ($\theta_M = 0$). [(i) and (ii)] The maximum and minimum values of $\langle\alpha_{40}\rangle$ $(41 + 5\sqrt{57})/112 \approx 0.7031$ and $(41 - 5\sqrt{57})/112) \approx 0.0290$, respectively, are achieved for $S = (1 - 3\sqrt{(19/3)})/2 \approx -0.7583$ and $S = (1+\sqrt{(19/3)})/2 \approx 1.758\,30$. (iii) The limiting value of $\langle\alpha_{40}\rangle$ for large S is 1/7. [(iv) and (v)] The maximum and minimum values of $\langle\alpha_{20}\rangle/\sqrt{5}$ $(R_L(0))$ correspond to $(4 + 9\sqrt{2})/28 \approx 0.5974$ and $(4 - 9\sqrt{2})/28 \approx -0.3117$ $S = -3+(2\sqrt{2}) \approx -0.0858$ and $S = -3 - (2\sqrt{2}) \approx -5.8284$. (vi) For large S, the limiting value of $\langle\alpha_{20}\rangle/\sqrt{5}$ is $-2/7$. (b) Variation in $\langle\alpha_{20}\rangle/\sqrt{5}$ and $\langle\alpha_{40}\rangle$ with D for TPA in which $S_{XX} = S_{YY}$ $(S = 1)$ where the emission transition dipole moment has equal projection on the molecular frame X and Y axes. (i) Maximum value of $\langle\alpha_{40}\rangle$ corresponding to $(41 + 5\sqrt{(57)})/112 \approx 0.7031$ at $D = (7 + \sqrt{(57)})/2$. (ii) Minimum value of $\langle\alpha_{40}\rangle = (41 - 5\sqrt{(57)})/112 \approx 0.029\,02$ with $D = (7 - \sqrt{(57)})/2$. (iii) Limiting value of $\langle\alpha_{40}\rangle$ at large $|D| = 38/56 \approx 0.0290$. The variation in $\langle\alpha_{20}\rangle/\sqrt{5}$ with D is less marked varying between maximum and minimum values of $(4 + \sqrt{2})/28$ (iv) and (v) $(4 - \sqrt{2})/28$ at $D = +\sqrt{2}$ and $-\sqrt{2}$, respectively. (vi) The limiting value of $\langle\alpha_{20}\rangle/\sqrt{5}$ at large $|D|$ (and $D = 0$) = 1/7.

Nd:YVO_4 (Verdi V-10, Coherent United Kingdom) pumped mode-locked Ti:sapphire laser (Mira 900F, Coherent United Kingdom). Fluorescence was detected using a polarized time correlated single photon counting (TCSPC) system described in detail elsewhere.[69] For compatibility with the TCPSC electronics, pulses were selected from the 76 MHz mode-locked pulse train at 4 MHz using an acousto-optic switch (Pulse select, APE Berlin Germany) and incident intensities were reduced to achieve a maximum count rate of 40 kHz to avoid pulse pile-up effects. A 90° excitation-detection geometry was employed with variable detection polarization as illustrated in Fig. 1. Linear excitation polarization was set using a Glan-Laser polarizer (Melles-Griot, USA). Circularly polarized excitation was achieved with linearly polarized light incident on a zero-order tunable quarter wave plate (Alphalas, Germany). Circular polarization was confirmed by observing rotation angle invariant transmission through a second (analyzing) linear polarizer. For the determination of Ω_{ABS}, the total emission resulting from each polarization was measured by running the TCSPC system in total counting mode for 10 s with the emission polarizer set at the appropriate magic angle [Figs. 1(a) and 1(b)]. This was repeated 5 times for each polarization to account for any drift in the laser excitation intensity, and an average ratio was calculated from the 10 values obtained from division of neighbouring intensities collected in the sequence. Fluorescence decays at detection polarizations parallel ($I_{||}$) and perpendicular ($I_\perp$) to the respective axis of cylindrical symmetry [Figs. 1(c) and 1(d)] were acquired by controlling the emission polarizer with a stepper motor. Vertically and horizontally polarized emission was alternately transmitted every 10 s for 5 min and the decays were stored separately in computer memory. Intensity and anisotropy decays were then reconstructed from the polarized fluorescence decays using

$$I(t) = I_{||}(t) + 2I_\perp(t), \tag{59}$$

$$R(t) = \frac{I_{||}(t) - I_\perp(t)}{I_{||}(t) + 2I_\perp(t)}. \tag{60}$$

This resulted in fluorescence intensity decays consisting of approximately 10^7 photons, with more than 10^5 photons in the peak channel. In addition to fluorescence intensity and anisotropy decays following linear and circularly polarized TPA, linearly polarized single-photon excitation of EGFP was undertaken at 490 nm close to the maximum of the $S_0 \rightarrow S_1$ transition using the 4 MHz output of an amplified frequency-doubled diode laser (PicoTA, PicoQuant). Decay times and amplitudes were extracted from the measured I(t) and R(t) curves using weighted least squares fitting in OriginPro 2015 (OriginLab) to minimise the $\chi_R{}^2$ statistic, given by

$$\chi_r^2 = \frac{1}{n-l}\sum_{k=1}^{n}\frac{1}{\sigma(t_k)^2}[N_{\text{measured}}(t_k) - N_{\text{model}}(t_k)]^2, \tag{61}$$

where n is the total number of time bins, $N_{\text{measured}}(t_k)$ is the experimental data in time bin t_k, and $N_{\text{model}}(t_k)$ is the value of the model function at this point, containing l freely varying parameters. σ_k is the expected standard deviation of the experimental data from the model at time t, obtained by propagating the known standard deviations of the independent Poisson random variables $I_{||}$ and $I_\perp$ through Eqs. (59) and (60), giving

$$\sigma_I(t_k)^2 = I_{||}(t_k) + 4I_\perp(t_k), \tag{62}$$

$$\sigma_R(t_k)^2 = \frac{I(t_k)^2}{(I_{||}(t_k) + 4I_\perp(t_k))\,R(t_k)^2 - 2\,(I_{||}(t_k) - 2I_\perp(t_k))\,R(t_k) + I_{||}(t_k) + I_\perp(t_k)}. \tag{63}$$

$\chi_R{}^2$ values below 2 were considered acceptable. Uncertainties in the fitting parameters were provided by support plane analysis performed by the fitting software. S and D were calculated from the three simultaneous equations for Ω_{ABS}, $R_L(0)$, and $R_C(0)$ [Eqs. (24), (41), and (42)], solving them numerically for $\theta_M = 0°$ and 5.5° using MATLAB (Mathworks United Kingdom). In order to calculate errors in the obtained S and D values, arising from uncertainties in Ω_{ABS}, $R_L(0)$, and $R_C(0)$, the equations were solved 5000 times using values randomly selected from Gaussian distributions of each parameter, centred on the obtained value with standard deviations equal to the associated error. The final S and D values were taken as the mean values of the 5000 obtained, with the standard deviation of these used for the quoted uncertainty.

IV. RESULTS AND DISCUSSION

A. Transition dipole moment orientation in EGFP

The anisotropy decays of EGFP for both single- [Fig. 3(a)] and two-photon [Fig. 3(b)] linearly polarized excitation were well described by single exponential fits, with rotational correlation times of 18.1 (±0.2) ns at 490 nm and 19.51 (±0.1) ns at 800 nm. The initial (t = 0) anisotropies, at 0.3945 (±0.0005) and 0.5520 (±0.0005) for single-photon and two-photon excitation, respectively, were close to the conventional theoretical limits of 0.4 and 0.571, suggesting only a small angle between the absorption and emission transition dipole moments. As fluorescence following single- and two-photon excitation of fluorescent proteins originates from the S_1 electronic state,[34,70] the emission transition dipole moment is a common molecular frame reference point. In single-photon excitation, the angle θ_{AE} between the absorption and emission transition dipole moment directions is given by the well known relation[43]

$$R(0) = \frac{0.4}{2}\left(3\cos^2\theta_{AE} - 1\right). \tag{64}$$

In a molecular frame coordinate system in which the absorption transition dipole moment $\mu^{ABS}_{S_0\rightarrow S_1}$ defines the molecular X axis, θ_{AE} and θ_M are equivalent[43] and $\theta_M = 5.5\ (\pm 0.3)°$. Recent theoretical calculations have determined $\mu^{ABS}_{S_0\rightarrow S_1}$ to be directed at 73° to the carbonyl group of the fluorescent protein chromophore[71] as illustrated in Fig. 4. Here the principal component of the transition tensor S_{XX} lies along $\mu^{ABS}_{S_0\rightarrow S_1}$. The alternative representation of the transition tensor would be to take X as the direction of the emission transition dipole moment $\mu^{EM}_{S_1\rightarrow S_0}$, here $\theta_M = 0°$, as depicted in Figs. 4(b) and 4(c).

The rotational diffusion times in aqueous solution of both recombinant EGFP[20] and wild-type GFP[18,33] following two-photon excitation have previously been measured as 17 ± 1 ns. For both linear and circularly polarized two-photon excitation at 800 nm, we observe single exponential decays with rotational correlation times of around 19 ns [Figs. 3(b) and 3(c)]. Non-equivalence of rotational correlation times following linear and circularly polarized two-photon excitation has been identified by Johnson and co-workers as indicative of significant off-diagonal transition tensor elements[33] with longer decay times reported for circularly polarized two-photon excitation in perylene where S_{XY} is of a similar magnitude to S_{XX} ($D \approx 0.87$).[33] The near equivalence of the rotational correlation times for linearly and circularly polarized two-photon excitation observed here for EGFP suggests that the contribution of off-diagonal elements (D) to the transition tensor is small.[43] Full calculation of S and D across the two-photon resonance of EGFP using the measurements performed here will confirm whether this is the case.

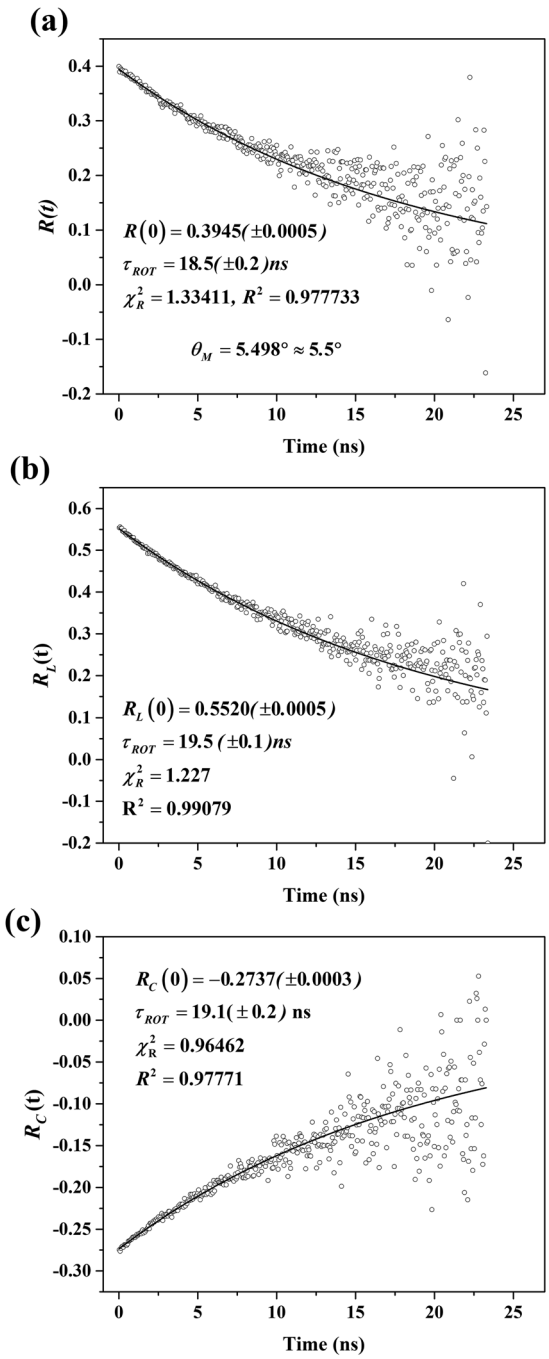

FIG. 3. (a) Fluorescence anisotropy decay of EGFP following single-photon excitation at 490 nm at the peak of the $S_0 \rightarrow S_1$ transition. (b) Fluorescence anisotropy decay of EGFP resulting from linearly polarized two-photon excitation at 800 nm. (c) Fluorescence anisotropy arising from circularly polarized two-photon excitation of EGFP at 800 nm.

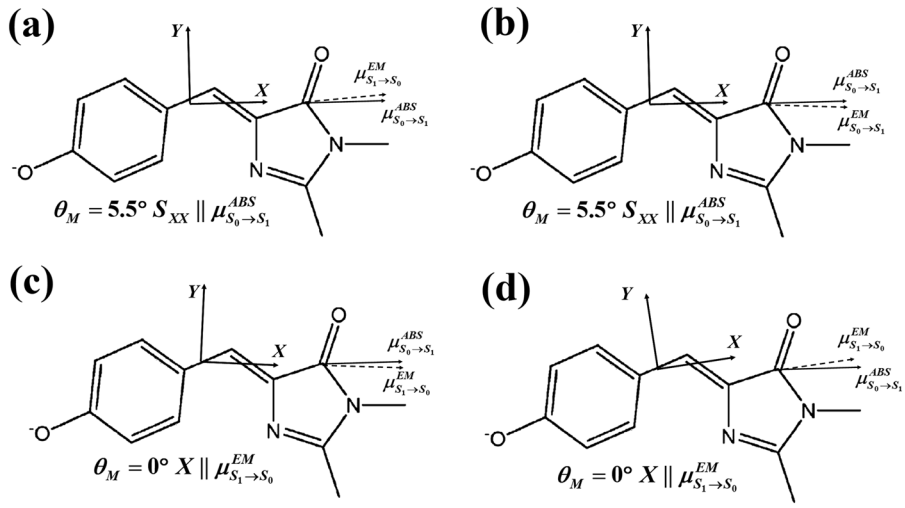

FIG. 4. Transition tensor coordinate systems for EGFP. The $S_0 \rightarrow S_1$ transition dipole moment in EGFP makes an angle of 73° to the carbonyl group. From single-photon anisotropy measurements (Fig. 3), the $S_1 \rightarrow S_0$ transition dipole moment is found to be oriented at an angle of 5.5° to this direction. Taking $\mu^{ABS}_{S_0 \rightarrow S_1}$ to define the direction of the principal element of the transition tensor (S_{XX}) corresponds to $\theta_M = 5.5°$. Fluorescence anisotropy measurements do not distinguish between positive and negative values of θ_M and both possibilities for the emission transition dipole moment orientation in the molecular frame are shown in (a) and (b). If S_{XX} is parallel to $\mu^{EM}_{S_1 \rightarrow S_0}$, $\theta_M = 0°$ and the coordinate system for the transition tensor can take two orientations in the molecular frame at angles of 78.5° and 67.5° to the carbonyl group [(c) and (d), respectively].

B. Two-photon tensor structure

The values of $R_C(0)$, $R_L(0)$, Ω_{ABS}, τ^{ROT}_{CIRC}, and τ^{ROT}_{LIN} at excitation wavelengths between 800 and 900 nm, together with the S and D values calculated for $\theta_M = 5.5°$ and 0°, are set out in Table III. $R_C(0)$, $R_L(0)$, and Ω_{ABS} show little variation with excitation wavelength as can be seen in Fig. 5, where they are plotted alongside the two-photon action cross section measurements of Drobizhev *et al.*[34,72] The fluorescence intensity decays following linearly and circularly polarized excitation are both well described by bi-exponential fitting as previously observed for single- and two-photon excitation of recombinant EGFP.[12,28,31] To within experimental error, both excitation processes yield identical amplitude weighted average decay times of 2.7-2.8 ns as shown in Table IV and Fig. 6.

As shown in Fig. 7, S_{XX} is seen to be dominant for both angles across all excitation wavelengths with S on the order of 10^{-2}. The contribution of off diagonal elements is reduced by a factor of approximately 2 when $\theta_M = 5.5°$. In both coordinate systems, D follows an approximately linear decrease with increasing excitation wavelength, reaching zero, within

TABLE III. Polarized TPA and fluorescence measurements and the calculated transition tensor structure parameters.

Excitation wavelength (nm)	$R_L(0)$	τ^{ROT}_{LIN} (ns)	$R_C(0)$	τ^{ROT}_{CIRC} (ns)	Ω	S $\theta_M = 0°$	D $\theta_M = 0°$	S $\theta_M = 5.5°$	D $\theta_M = 5.5°$
800	0.5520 ± 0.0005	19.5 ± 0.1	−0.2737 ± 0.0003	19.1 ± 0.2	0.67 ± 0.01	0.03 ± 0.01	0.18 ± 0.04	0.009 ± 0.009	0.010 ± 0.007
	$\chi_R^2 = 1.227$		$\chi_R^2 = 0.965$						
820	0.5557 ± 0.0004	19.3 ± 0.1	−0.2796 ± 0.0003	19.6 ± 0.1	0.66 ± 0.05	0.03 ± 0.05	0.13 ± 0.06	−0.10 ± 0.05	0.07 ± 0.02
	$\chi_R^2 = 1.075$		$\chi_R^2 = 1.012$						
840	0.5568 ± 0.0006	18.4 ± 0.1	−0.2755 ± 0.0003	18.5 ± 0.2	0.67 ± 0.02	0.02 ± 0.02	0.16 ± 0.04	0.00 ± 0.02	0.068 ± 0.007
	$\chi_R^2 = 1.021$		$\chi_R^2 = 0.965$						
860	0.5595 ± 0.0006	19.1 ± 0.1	−0.2768 ± 0.0004	19.5 ± 0.2	0.63 ± 0.03	0.04 ± 0.03	0.14 ± 0.05	0.03 ± 0.03	0.05 ± 0.01
	$\chi_R^2 = 1.200$		$\chi_R^2 = 1.112$						
880	0.5633 ± 0.0005	19.1 ± 0.1	−0.2807 ± 0.0003	19.2 ± 0.2	0.658 ± 0.007	0.032 ± 0.008	0.11 ± 0.02	0.012 ± 0.006	0.011 ± 0.007
	$\chi_R^2 = 1.218$		$\chi_R^2 = 1.063$						
900	0.5617 ± 0.0003	19.2 ± 0.1	−0.2806 ± 0.0003	19.3 ± 0.1	0.67 ± 0.02	0.03 ± 0.02	0.10 ± 0.04	−0.03 ± 0.02	0.005 ± 0.008
	$\chi_R^2 = 1.086$		$\chi_R^2 = 0.993$						

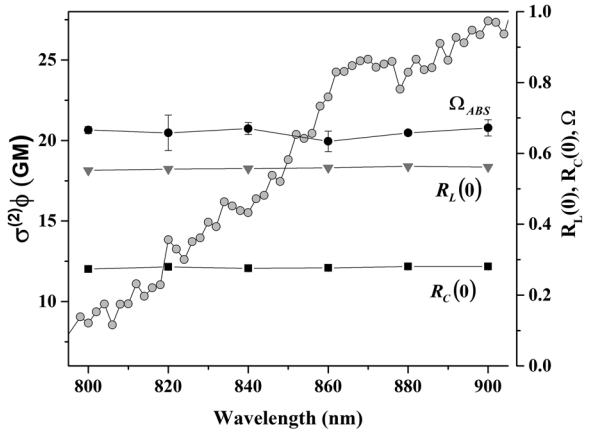

FIG. 5. Structure determining parameters $R_L(0)$, $R_C(0)$, and Ω_{ABS} as a function of two-photon excitation wavelength, overlaid with two-photon action cross section measurements $\sigma^{(2)}\phi$ of Drobizhev *et al.*[34]

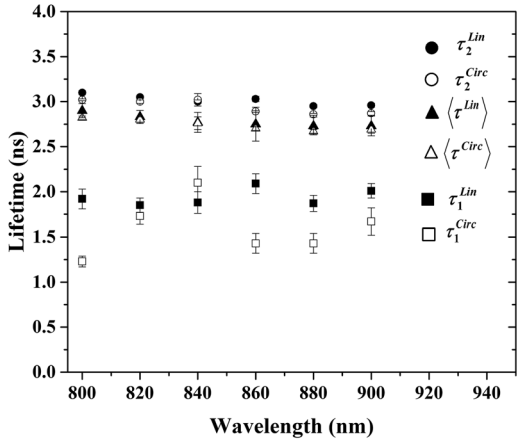

FIG. 6. Bi-exponential fluorescence decay parameters obtained for EGFP following linearly and circularly polarized two-photon excitation. With both excitation polarizations, the longer lifetime τ_2 is the majority decay component. This and the average (amplitude weighted) fluorescence lifetime $\langle\tau\rangle$ show little wavelength variation.

experimental uncertainty, at 900 nm for $\theta_M = 5.5°$. The uncertainties in D with this representation of the transition tensor are also notably smaller. Two-photon absorption between 800 and 900 nm in EGFP is clearly dominated by a single diagonal element (S_{XX}). Taking the single photon $S_0 \rightarrow S_1$ absorption transition moment $\mu^{ABS}_{S_0 \rightarrow S_1}$ to define the principal axis (X) in the molecular frame, the transition tensor is, to a good approximation, diagonal ($D \leq 0.1$ at 800 nm, tending to 0 at 900 nm) with $S \leq 0.001$ at most excitation wavelengths.

C. Assignment of two-photon transitions in EGFP

The two-photon absorption spectrum of fluorescent proteins consists of two electronic transitions separated by a distinct minimum. In the case of EGFP, this occurs at 700 nm with the long wavelength absorption maximum 930 nm.[34,45,46] This transition has been assigned to the lowest energy singlet state ($S_0 \rightarrow S_1$)[34] and that of the short-wavelength feature to a higher energy singlet state $S_0 \rightarrow S_n$.[73] Since the chromophores of fluorescent proteins do not possess a centre of symmetry, the parity selection rules for one- and two-photon transitions are relaxed.[34,45,46] Consequently, the same transitions should appear in both one- and two-photon absorption spectra although with different relative intensities. The notable blue shift in the long wavelength TPA absorption (930 nm) with respect to that for one-photon excitation (490 nm ≡ 980 nm) has been ascribed to the vibronic enhancement resulting from transitions terminating to higher vibrational levels in the S_1 manifold.[74,75] An alternative mechanism for two-photon absorption in EGFP assigns the long wavelength transition to the participation of a putative close lying S_2 state.[75] Our results indicate that S_{XX}, the principal component of the two-photon transition tensor in EGFP, has the same molecular frame orientation as the single-photon $S_0 \rightarrow S_1$ transition moment. This, together with the small and vanishing nature of the off-diagonal transition tensor elements as the excitation wavelength approaches the two-photon maximum [Fig. 7(b)],

TABLE IV. Two-photon fluorescence intensity decays recorded for (a) linearly and (b) circularly polarized excitation wavelengths from 800 to 900 nm.

(a) ↑↑λ (nm)	A_1	τ_1 (ns)	A_2	τ_2(ns)	$\langle\tau\rangle$ (ns)	χ^2_R
800	0.17 ± 0.02	1.9 ± 0.1	0.83 ± 0.02	3.10 ± 0.02	2.90 ± 0.03	1.50
820	0.18 ± 0.02	1.85 ± 0.08	0.82 ± 0.02	3.05 ± 0.01	2.83 ± 0.03	1.38
840	0.20 ± 0.03	1.9 ± 0.1	0.80 ± 0.03	3.00 ± 0.02	2.78 ± 0.04	1.45
860	0.29 ± 0.05	2.1 ± 0.1	0.71 ± 0.05	3.03 ± 0.03	2.76 ± 0.05	1.40
880	0.21 ± 0.02	1.87 ± 0.09	0.79 ± 0.03	2.95 ± 0.02	2.73 ± 0.03	1.53
900	0.25 ± 0.03	2.01 ± 0.08	0.75 ± 0.03	2.96 ± 0.02	2.72 ± 0.03	1.63
(b) ↻↺ λ (nm)	A_1	τ_1 (ns)	A_2	τ_2 (ns)	$\langle\tau\rangle$ (ns)	χ^2_R
800	0.11 ± 0.01	1.23 ± 0.06	0.89 ± 0.01	3.02 ± 0.01	2.82 ± 0.02	1.33
820	0.16 ± 0.02	1.73 ± 0.09	0.84 ± 0.02	3.00 ± 0.02	2.80 ± 0.03	1.33
840	0.3 ± 0.1	2.1 ± 0.2	0.7 ± 0.1	3.02 ± 0.07	2.76 ± 0.07	1.99
860	0.13 ± 0.01	1.4 ± 0.1	0.87 ± 0.02	2.89 ± 0.01	2.70 ± 0.02	1.25
880	0.13 ± 0.01	1.4 ± 0.1	0.87 ± 0.02	2.86 ± 0.01	2.67 ± 0.02	1.51
900	0.15 ± 0.03	1.7 ± 0.2	0.85 ± 0.03	2.87 ± 0.02	2.69 ± 0.04	1.41

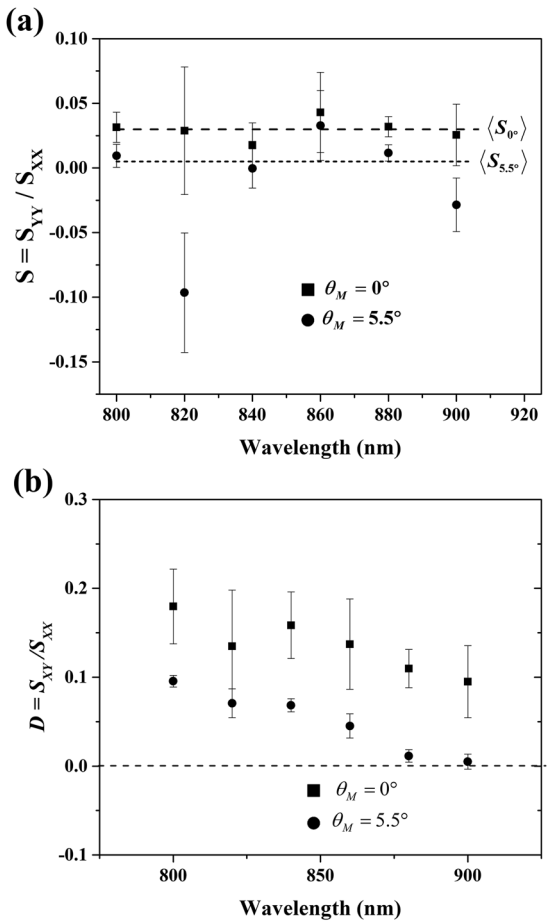

FIG. 7. Variation in the transition tensor structure with two-photon excitation wavelength. (a) Taking $\mu^{ABS}_{S_0\rightarrow S_1}$ to be the molecular frame X axis as implied by fluorescence anisotropy data (Fig. 5), S is minimised. Neglecting the data points at 820 nm which have large associated errors, the average values of S for the two representations across the excitation wavelengths are 0.030 ($\theta_M = 0°$) and 0.005 ($\theta_M = 5.5°$). (b) The degree of off-diagonal elements $D = D_{XY}/D_{XX}$ for both molecular axis systems shows a decrease as the excitation wavelengths approach the near infrared two-photon absorption maximum at 930 nm. The values obtained in the $\mu^{ABS}_{S_0\rightarrow S_1}$ axis system are, however, consistently lower, the disparity growing with increasing excitation wavelength. The value of D obtained at 900 nm is, to within experimental error, zero.

further reinforces the conclusion that the transition has the same symmetry as the squared modulus of the $S_0 \rightarrow S_1$ transition dipole moment. Whilst these observations do not disprove the participation of another electronic state in the two-photon transition, they are however fully consistent with the current $S_0 \rightarrow S_1$ assignment. The participation of a close-lying S_2 state has recently been argued from solvent shifts in TPA.[75] In this light, it would be instructive if broad spectrum linearly and circularly polarized two-photon absorption and fluorescence anisotropy measurements were performed to augment such data. Solvent effects in two-photon absorption have been investigated theoretically and experimentally by Wirth and co-workers[76,77] through two-photon absorption anisotropy measurements. An extension of this approach to include linearly and circularly polarized fluorescence observables and the measurement of the higher order moments that are unavoidably prepared by two-photon absorption would provide additional and perhaps more sensitive information as to the nature of two-photon transitions in fluorescent proteins.

TABLE V. Values of the initial hexadecapolar alignment predicted from Ω_{ABS}, $R_C(0)$, and $R_L(0)$ measurements for emission transition dipole alignment angles $\theta_M = 0°$ and 5.5°.

Excitation wavelength (nm)	$\langle\alpha_{40}\rangle$ $\theta_M = 0°$	$\langle\alpha_{40}\rangle$ $\theta_M = 5.5°$
800	0.32 ± 0.02	0.381 ± 0.006
820	0.34 ± 0.04	0.44 ± 0.03
840	0.34 ± 0.02	0.38 ± 0.01
860	0.33 ± 0.02	0.36 ± 0.02
880	0.347 ± 0.007	0.361 ± 0.004
900	0.35 ± 0.02	0.38 ± 0.01

D. Hexadecapolar alignment: Initial values and predicted relaxation rates

Using the calculated values of S and D, we can determine [Eq. (56)] the values of $\langle\alpha_{40}\rangle$ for $\theta_M = 0$ and 5.5° as a function of excitation wavelength. These are set out in Table V and plotted in Fig. 8. When S_{XX} is collinear to the $S_0 \rightarrow S_1$ transition dipole moment ($\theta_M = 5.5°$), the predicted values of

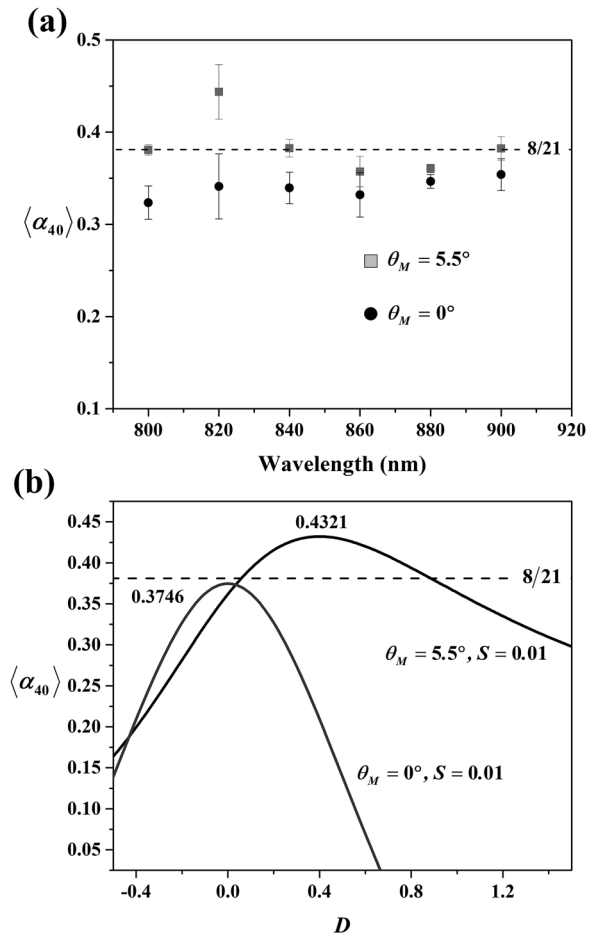

FIG. 8. (a) Predicted hexadecapolar alignment created by two-photon absorption in EGFP using the measured S and D values for emission transition dipole moment angles obtained for a single-element transition tensor with a parallel emission transition dipole moment. (b) Variation in $\langle\alpha_{40}\rangle$ with D for $\theta_M = 0°$ and 5.5° and $S = 0.01$. For $\theta_M = 0°$, $\langle\alpha_{40}\rangle < 8/21$ for all values of D. If $\theta_M = 5.5°$ with D values between 0.06 and 0.80, $\langle\alpha_{40}\rangle > 8/21$.

$\langle\alpha_{40}\rangle$ lie above 8/21, the theoretical value achieved by a single-element transition tensor with a parallel emission transition dipole moment. For $\theta_M = 0°$, the increased contribution of off diagonal elements D yields values of $\langle\alpha_{40}\rangle$ that are consistently below 8/21.

Using polarized time-resolved STED with a variable delay between excitation (pump) and depletion (dump) pulses, it is possible to measure the time evolution of $\langle\alpha_{40}\rangle$.[38,59] With small step isotropic rotational diffusion, the K = 2 and K = 4 alignment relaxation rates follow single exponential decay dynamics[49] with the K = 2 and K = 4 rotational correlation times for a symmetric diffuser related by

$$\tau_{20}^{ROT} = \frac{10}{3}\tau_{40}^{ROT}. \tag{65}$$

The rotational diffusion time of EGFP following linearly polarized two-photon excitation yields values in the region of 19 ns. We might therefore expect τ_{40}^{ROT} to be approximately 5.4 ns with an initial value of $\langle\alpha_{40}\rangle$ close to that of 8/21 from the S and D values obtained using the $\mu_{S_0\rightarrow S_1}^{ABS}$ axis system. The greater sensitivity of $\langle\alpha_{40}\rangle$ to transition dipole moment reorientation arising from small step rotational diffusion is also expected to be mirrored in other depolarization mechanisms such as homo-FRET.[78] The development of time-resolved STED techniques for investigating these dynamics will be the subject of the companion paper.[57]

V. CONCLUSIONS

We have developed the necessary theoretical framework for the full characterization of molecular transition dipole alignment following two-photon excitation. We have used this formalism with measurements of the linearly and circularly polarized two-photon absorption anisotropy and time resolved fluorescence anisotropy to determine the structure of the two-photon transition tensor of EGFP and to predict the degree of hexadecapolar alignment that is created in two-photon absorption but not observed via spontaneous emission. For excitation wavelengths spanning 800 nm to 900 nm, the EGFP transition tensor possesses a dominant single element (S_{XX}) and is most close to diagonal if this has the same molecular frame orientation as the single photon $S_0 \rightarrow S_1$ transition dipole moment. These observations are in line with the assignment of the near infra-red two photon absorption as a vibronically enhanced $S_0 \rightarrow S_1$ transition.[34,45,46] The sensitivity of $\langle\alpha_{40}\rangle$ to the underlying structure of the two-photon transition tensor and the molecular frame orientation of the emission transition dipole moment is seen to be marked, providing complimentary information to polarized absorption and fluorescence measurements. These results highlight the importance of the development of methods to measure this hitherto "hidden" degree of excited state alignment.

ACKNOWLEDGMENTS

We are grateful to the Engineering and Physical Sciences Research Council for financial support of this work through Ph.D. studentships awarded to T.A.M. and T.S.B. via the CoMPLEX doctoral training centre at UCL. The two-photon action cross section data for EGFP in Fig. 5 were kindly provided by Mikhail Drobizhev. We would like to thank Sara Kisakye-Nambozo and Svend Kjaer (Cancer Research United Kingdom, Lincoln's Inn Fields) for their help in the preparation and purification of recombinant EGFP.

[1] O. Shimomura, F. H. Johnson, and Y. Saiga, J. Cell. Comp. Physiol. **59**, 223 (1962).
[2] R. Y. Tsien, Annu. Rev. Biochem. **67**, 509 (1998).
[3] M. Zimmer, Chem. Rev. **102**, 759 (2002).
[4] G. H. Patterson, S. M. Knobel, W. D. Sharif, S. R. Kain, and D. W. Piston, Biophys. J. **73**, 2782 (1997).
[5] O. Thastrup, S. Tullin, L. K. Poulsen, and S. P. Bjørn, U.S. patent 6,172,188 (9 January 2001).
[6] T.-T. Yang, P. Sinai, G. Green, P. A. Kitts, Y.-T. Chen, L. Lybarger, R. Chervenak, G. H. Patterson, D. W. Piston, and S. R. Kain, J. Biol. Chem. **273**, 8212 (1998).
[7] B. P. Cormack, R. H. Valdivia, and S. Falkow, Gene **173**, 33 (1996).
[8] M. Xian, N. Honbo, J. Zhang, C.-C. Liew, J. S. Karliner, and Y.-F. C. Lau, J. Mol. Cell. Cardiol. **31**, 2155 (1999).
[9] A. Miyawaki, J. Llopis, R. Heim, and J. M. McCaffery, Nature **388**, 882 (1997).
[10] V. Calleja, D. Alcor, M. Laguerre, J. Park, B. Vojnovic, B. A. Hemmings, J. Downward, P. J. Parker, and B. Larijani, PLoS Biol. **5**, e95 (2007).
[11] B. D. Slaughter, J. W. Schwartz, and R. Li, Proc. Natl. Acad. Sci. U. S. A. **104**, 20320 (2007).
[12] T. A. Masters, V. Calleja, D. A. Armoogum, R. J. Marsh, C. J. Applebee, M. Laguerre, A. J. Bain, and B. Larijani, Sci. Signaling **3**, ra78 (2010).
[13] W. Denk, J. H. Strickler, and W. W. Webb, Science **248**, 73 (1990).
[14] W. Denk and K. Svoboda, Neuron **18**, 351 (1997).
[15] W. R. Zipfel, R. M. Williams, and W. W. Webb, Nat. Biotechnol. **21**, 1369 (2003).
[16] A. J. Bain and A. J. McCaffery, Chem. Phys. Lett. **108**, 275 (1984).
[17] S.-Y. Chen and B. W. Van Der Meer, Biophys. J. **64**, 1567 (1993).
[18] C. Wan and C. K. Johnson, Chem. Phys. **179**, 513 (1994).
[19] P. R. Callis, J. Chem. Phys. **99**, 27 (1993).
[20] A. Volkmer, V. Subramaniam, D. J. S. Birch, and T. M. Jovin, Biophys. J. **78**, 1589 (2000).
[21] N. Chadborn, J. Bryant, A. J. Bain, and P. O'Shea, Biophys. J. **76**, 2198 (1999).
[22] C. W. Ko, Z. Wei, R. J. Marsh, D. A. Armoogum, N. Nicolaou, A. J. Bain, A. Zhou, and L. Ying, Mol. Biosyst. **5**, 1025 (2009).
[23] M. Van Zandvoort, H. C. Gerritsen, G. Van Ginkel, Y. K. Levine, R. Tarroni, and C. Zannoni, J. Phys. Chem. B **101**, 4149 (1997).
[24] A. Gidwani, D. Holowka, and B. Baird, Biochemistry **40**, 12422 (2001).
[25] P. Ferrand, P. Gasecka, A. Kress, X. Wang, F.-Z. Bioud, J. Duboisset, and S. Brasselet, Biophys. J. **106**, 2330 (2014).
[26] R. E. Dale and J. Eisinger, Biopolymers **13**, 1573 (1974).
[27] F. Tanaka and N. Mataga, Photochem. Photobiol. **29**, 1091 (1979).
[28] T. A. Masters, R. J. Marsh, D. A. Armoogum, N. Nicolaou, B. B. Larijani, and A. J. Bain, J. Am. Chem. Soc. **135**, 7883 (2013).
[29] S. S. White, H. Li, R. J. Marsh, J. D. Piper, N. D. Leonczek, N. Nicolaou, A. J. Bain, L. Ying, and D. Klenerman, J. Am. Chem. Soc. **128**, 11423 (2006).
[30] A. A. Heikal, S. T. Hess, and W. W. Webb, Chem. Phys. **274**, 37 (2001).
[31] S. T. Hess, E. D. Sheets, A. Wagenknecht-Wiesner, and A. A. Heikal, Biophys. J. **85**, 2566 (2003).
[32] A. J. W. G. Visser, S. P. Laptenok, N.V. Visser, A. van Hoek, D. J. S. Birch, J.-C. Brochon, and J. W. Borst, Eur. Biophys. J. **39**, 241 (2010).
[33] S. W. Pauls, J. F. Hedstrom, and C. K. Johnson, Chem. Phys. **237**, 205 (1998).
[34] M. Drobizhev, N. S. Makarov, S. E. Tillo, T. E. Hughes, and A. Rebane, Nat. Methods **8**, 393 (2011).
[35] A. J. Bain and A. J. McCaffery, J. Chem. Phys. **80**, 5883 (1984).
[36] A. J. Bain and A. J. McCaffery, J. Chem. Phys. **83**, 2627 (1985).
[37] A. J. Bain and A. J. McCaffery, J. Chem. Phys. **83**, 2641 (1985).
[38] A. J. Bain, P. Chandna, and J. Bryant, J. Chem. Phys. **112**, 10418 (2000).
[39] T. Tao, Biopolymers **8**, 609 (1969).
[40] D. Artigas, D. Merino, C. Polzer, and P. Loza-Alvarez, Optica **4**, 911 (2017).
[41] J. Lazar, A. Bondar, S. Timr, and S. J. Firestein, Nat. Methods **8**, 684 (2011).
[42] A. Gasecka, T.-J. Han, C. Favard, B. R. Cho, and S. Brasselet, Biophys. J. **97**, 2854 (2009).

[43]L. Ryderfors, E. Mukhtar, and L. B.-Å. Johansson, J. Phys. Chem. A **112**, 5794 (2008).
[44]A. J. Bain, *Polarised Laser Fluorescence Studies of Ground and Excited State Dynamics* (University of Sussex, 1984).
[45]G. A. Blab, P. H. M. Lommerse, L. Cognet, G. S. Harms, and T. Schmidt, Chem. Phys. Lett. **350**, 71 (2001).
[46]M. Drobizhev, S. Tillo, N. S. Makarov, T. E. Hughes, and A. Rebane, J. Phys. Chem. B **113**, 855 (2009).
[47]R. J. Marsh, D. A. Armoogum, and A. J. Bain, Chem. Phys. Lett. **366**, 398 (2002).
[48]A. J. Bain, R. J. Marsh, D. A. Armoogum, O. Mongin, L. Porrès, and M. Blanchard-Desce, Biochem. Soc. Trans. **31**, 1047 (2003).
[49]R. J. Marsh, N. D. Leonczek, D. A. Armoogum, E. M. Monge, and A. J. Bain, Proc. SPIE **5925**, 59250C-1–59250C-12 (2005).
[50]R. J. Marsh, N. D. Leonczek, D. A. Armoogum, L. Porres, O. Mongin, M. Blanchard-Desce, and A. J. Bain, Proc. SPIE **5510** (2004).
[51]D. A. Armoogum, R. J. Marsh, and A. J. Bain, Proc. SPIE **5222**, 34–44 (2003).
[52]D. A. Armoogum, R. J. Marsh, N. Nicolaou, O. Mongin, M. Blanchard-Desce, and A. J. Bain, Proc. SPIE **7030**, 70300S (2008).
[53]M. Bell, R. Dale, U. van der Heide, and Y. Goldman, Biophys. J. **83**, 1050 (2002).
[54]R. Swaminathan, C. Hoang, and A. Verkman, Biophys. J. **72**, 1900 (1997).
[55]M. Velez and D. Axelrod, Biophys. J. **53**, 575 (1988).
[56]W. A. Wegener, Biophys. J. **46**, 795 (1984).
[57]T. A. Masters, N. A. Robinson, R. J. Marsh, T. S. Blacker, D. A. Armoogum, B. Larijani, and A. J. Bain, J. Chem. Phys. **148**, 134312 (2018).
[58]A. J. Bain, *Photonics* (John Wiley & Sons, Inc., Hoboken, NJ, USA, 2015), pp. 279–320.
[59]A. J. Bain, *An Introduction to Laser Spectroscopy* (Springer US, Boston, MA, 2002), pp. 171–210.
[60]A. J. Bain, P. Chandna, G. Butcher, and J. Bryant, J. Chem. Phys. **112**, 10435 (2000).
[61]W. M. McClain and R. A. Harris, Excited States **3**, 1 (1977).
[62]J. M. Leeder and D. L. Andrews, J. Chem. Phys. **134**, 03B602 (2011).
[63]W. M. McClain, J. Chem. Phys. **58**, 324 (1973).
[64]D. M. Brink and G. R. Satchler, *Angular Momentum* (Clarendon Press, 1968).
[65]P. R. Callis, T. W. Scott, and A. C. Albrecht, J. Chem. Phys. **75**, 5640 (1981).
[66]P. R. Callis, Annu. Rev. Phys. Chem. **48**, 271 (1997).
[67]J. A. J. Arpino, P. J. Rizkallah, and D. D. Jones, PLoS One **7**, e47132 (2012).
[68]A. Royant and M. Noirclerc-Savoye, J. Struct. Biol. **174**, 385 (2011).
[69]T. S. Blacker, R. J. Marsh, M. R. Duchen, and A. J. Bain, Chem. Phys. **422**, 184 (2013).
[70]M. Kasha, Discuss. Faraday Soc. **9**, 14 (1950).
[71]T. Ansbacher, H. K. Srivastava, T. Stein, R. Baer, M. Merkx, and A. Shurki, Phys. Chem. Chem. Phys. **14**, 4109 (2012).
[72]M. Drobizhev, personal communication (2013).
[73]M. Drobizhev, N. S. Makarov, T. Hughes, and A. Rebane, J. Phys. Chem. B **111**, 14051 (2007).
[74]H. Hosoi, S. Yamaguchi, H. Mizuno, A. Miyawaki, and T. Tahara, J. Phys. Chem. B **112**, 2761 (2008).
[75]H. Hosoi, R. Tayama, S. Takeuchi, and T. Tahara, Chem. Phys. Lett. **630**, 32 (2015).
[76]M. J. Wirth, A. C. Koskelo, and C. E. Mohler, J. Phys. Chem. **87**, 4395 (1983).
[77]C. E. Mohler and M. J. Wirth, J. Chem. Phys. **88**, 7369 (1988).
[78]F. T. S. Chan, C. F. Kaminski, and G. S. Kaminski Schierle, ChemPhysChem **12**, 500 (2011).